Hindawi
Shock and Vibration
Volume 2023, Article ID 6653564, 12 pages
https://doi.org/10.1155/2023/6653564

Research Article

Study on Preload of Bolted Connections in Pitch Bearing Based on Vibration Modal Analysis

Hongwei Zhang,[1] **Tao Chen**,[1] **Kangkang Ji**,[1] **Meng Zhu**,[1] **and Chengwei Ju**[2]

[1]*School of Mechanical Engineering, Beijing Institute of Petrochemical Technology, Beijing 102617, China*
[2]*Guangxi Special Equipment Inspection and Research Institute, Nanning 530299, China*

Correspondence should be addressed to Chengwei Ju; 13707880178@163.com

Received 10 July 2023; Revised 18 September 2023; Accepted 20 September 2023; Published 7 October 2023

Academic Editor: Marco Civera

In wind turbine systems, bolted connections are frequently subjected to gravitational and centrifugal loads transmitted by the blades during operation. This can lead to the attenuation of bolt preloading, resulting in bolt loosening or uneven loading, which in turn affects the service life of the generator unit. Therefore, the study of bolt preloading variations is crucial. However, there are numerous factors influencing bolt preloading, and the existing techniques struggle to precisely assess bolt preloading. This paper proposed a bolt preloading evaluation technique based on the hammer modal method. Focusing on the 42CrMo4 bolted connection of a pitch bearing, a test platform for bolt preloading assessment is constructed. Hammer modal tests are conducted under various preloading forces. By combining finite element modal analysis, the correspondence between preloading changes and the bending frequencies and modes of the bolted connection is obtained. The research illustrated that with changes in bolt preloading, variations occur in coherence, phase, and natural frequencies of frequency response functions. The fundamental correlation between bolt preloading and the second-order bending frequency can be utilized to assess changes in preloading. Furthermore, the applicability of this method has been validated, offering a reference for evaluating bolt preloading.

1. Introduction

The pitch bearing in a wind turbine, as one of the essential components, serves to connect the hub and blades, working in conjunction with the pitch drive system to adjust the angle of the blades for wind power generation. During the operation of a wind turbine, the bolted connection of the pitch bearing is subjected to gravitational loads transmitted by the blades, centrifugal loads, and torque from the drive gear. These factors can significantly reduce the bolt preload, leading to phenomena such as bolt loosening or uneven loading, exacerbating fatigue wear of the pitch bearing. Over prolonged operation, bolt connection failures can occur, affecting the entire turbine's overall safety, reliability, and lifespan [1–5]. Therefore, the assessment of bolt preload is of paramount importance.

Currently, hammer impact tests, torque tests, and ultrasonic tests are the main methods used for evaluating preload. Traditional hammer impact tests rely on the subjective judgment of testing personnel based on the characteristic sound emitted by the vibration device, but they do not provide quantitative monitoring. Torque tests control bolt preload by using a torque wrench, but this method is mainly applicable to later-stage equipment maintenance and is challenging to accurately evaluate axial forces due to the changing friction characteristics of the contact surfaces with tightening. Ultrasonic testing for bolt preload primarily involves measuring the sound propagation delay of the bolt head [6–9], the ratio of longitudinal and transverse wave velocities [10–13], combined vibration modes and longitudinal ultrasonic waves [14], or the shift in resonance frequency [15–18]. Due to the numerous factors influencing bolt preload, the above methods have certain errors. Therefore, to address this issue, the most advanced technique currently is to directly measure preload by embedding strain gauges and fiber optic grating sensors into the bolts. However, this method has limitations in bolt

connection devices and is cost-intensive [19–21]. Literature [22–24] has shown through simulation and experimental methods that the magnitude of preload can alter the natural frequency of the connected components, with greater preload resulting in increased natural frequency, providing a reference for testing residual bolt preload. Zhang [25] established stiffness and finite element models for bolted CFRP (carbon fiber reinforced polymer) lap joints and quantitatively calculated bolt relaxation position and residual preload using artificial neural network algorithms. The results indicated a positive correlation between the bolt's third-order bending mode and bolt preload. Hou [26], starting from the microlevel perspective of the bolt contact surface, studied the influence of contact stiffness and damping on the dynamic characteristics of bolted connections. Through mutual verification using hammer vibration tests and modal simulations, the modal damping ratio under different preloads was obtained, indicating that modal damping increases with increasing bolt preload.

This paper presented a method for assessing bolt preloading based on vibration modal analysis. A testing platform for evaluating bolt preloading was established and hammer modal tests on 42CrMo4 bolted connections of pitch bearings under various preloading conditions were conducted. By integrating finite element modal analysis and harmonic response, the changes in bending frequencies and modes of bolted connections under different preloading forces were analyzed. The evaluation of preloading variations was conducted based on the bending frequencies. Furthermore, the method was validated through hammer modal tests on bolted connections with varying dimensions and sizes.

2. Modal Experiment Principle

To obtain a feasible method for effectively monitoring the preloading force of bolts, the concept of smart washers as an elastic suspension cantilever, as proposed by Okugawa and Egawa [27], was considered. It was found that when the clamping force on the smart washer was sufficiently high, its natural frequency was the same as when fully tightened. As the clamping force decreased, the natural frequency of the smart washer decreased, allowing the clamping status to be monitored by detecting changes in the natural frequency. Therefore, the bolted connection could be regarded as a cantilever with an elastic suspension consisting of translational and rotational springs. The reduction in preloading force resulted in a decrease in the stiffness of the bolted connection, which was reflected in changes in the natural frequency. By conducting modal testing to measure the natural frequencies and mode shapes of the bolted connection structure, the preloading force could be effectively assessed.

Modal parameters, including frequency, mode shape, and damping ratio, were intrinsic characteristics of the structure and could be obtained through modal analysis [28]. Modal testing involves analyzing the continuous physical signals obtained from the test and expressing the dynamic properties of any structure using an Nth-order differential equation [26].

$$M\ddot{x} + C\dot{x} + Kx = f(t), \tag{1}$$

$$\left[\mathrm{Ms}^2 + \mathrm{Cs} + K\right]X(s) = F(s), \tag{2}$$

$$Z(s) = \left[\mathrm{Ms}^2 + \mathrm{Cs} + K\right]. \tag{3}$$

Equation (3) was the dynamic matrix of the structure, expressing the frequency response characteristics. The frequency response function matrix was its inverse matrix, which is as follows:

$$H(s) = \left[\mathrm{Ms}^2 + \mathrm{Cs} + K\right]^{-1}. \tag{4}$$

Therefore, $X(s)$ is expressed as follows:

$$X(s) = H(s)F(s). \tag{5}$$

Let $s = j\omega$; equation (5) gave the relationship between the excitation response and the excitation input as follows:

$$X(j\omega) = H(j\omega)F(j\omega). \tag{6}$$

The frequency response function matrix is as follows:

$$H_{ij}(\omega) = \frac{X_i(\omega)}{F_i(\omega)}. \tag{7}$$

It could be seen from the above formula that when there was only excitation in coordinate j, the frequency response of coordinate i was inversely proportional to the excitation force.

Similarly, the impedance matrix could be obtained from equation (3) as follows:

$$Z(\omega) = \left(k - \omega^2 M\right) + j\omega C. \tag{8}$$

The M and k matrices were weighted orthogonal to obtain the following equation:

$$\begin{aligned}
\Phi^T M \Phi &= \begin{bmatrix} m_1 & & \\ & m_r & \\ & & m_n \end{bmatrix}, \\
\Phi^T K \Phi &= \begin{bmatrix} k_1 & & \\ & k_r & \\ & & k_n \end{bmatrix}, \\
\Phi^T M \Phi &= \begin{bmatrix} m_1 & & \\ & m_r & \\ & & m_n \end{bmatrix}, \\
\Phi^T K \Phi &= \begin{bmatrix} k_1 & & \\ & k_r & \\ & & k_n \end{bmatrix}.
\end{aligned} \tag{9}$$

Therefore, the vibration mode matrix $\phi = [\phi_1, \phi_2, \cdots \phi_n]$; the damping matrix was orthogonal to the vibration mode matrix, and the following equation could be obtained:

$$\Phi^T C \Phi = \begin{bmatrix} c_1 & & \\ & c_r & \\ & & c_n \end{bmatrix}. \tag{10}$$

We brought the above formula into equation (8) to get the following equation:

$$Z(\omega) = \Phi^{-T} = \begin{bmatrix} c_1 & & \\ & c_r & \\ & & c_n \end{bmatrix} \Phi^{-1}. \tag{11}$$

The transfer function of the jointly obtained structure above is as follows:

$$H_{ij}(\omega) = \sum_{r=1}^{N} \frac{\Phi_{ri}\Phi_{rj}}{m_r\left[\left(\omega_r^2 - \omega^2\right) + j2\xi_r\omega_r\omega\right]}. \tag{12}$$

In the formula, $\omega_r^2 = k_r/m_r$, $\xi_r = c_r/2m_r\omega_r$, K is the stiffness matrix, k_r is the r-th order modal stiffness matrix, N is the total order of structural mode, $H_{ij}(\omega)$ is the transfer function of structure, m_r is the modal mass, Φ_{ri}, Φ_{rj} is the i and j r-order modal shape of i and j point, ω_r is the r-th modal frequency, and ξ_r is the damping ratio.

Based on Okugawa's study [22] on the testing method for the clamping force of smart washers, a frequency equation was established. By using equation (17), the correlation between the natural frequency of the bolt and the pretightening force could be determined. Therefore, the variation in the pretightening force of the bolt could be evaluated by testing the changes in the natural frequency of the bolted connection structure.

$$(\sin\beta l + \sin h\,\beta l)x_1 - (\cos\beta l + \cos h\,\beta l)x_2 + 2x_3 = 0, \tag{13}$$

$$2\frac{\mathrm{EI}\beta}{k_T}\cos\beta l - \sin\beta l + \sin h\,\beta l + \frac{\left(EI\beta^2\right)^2}{k_T k_R}(\sin\beta l + \sin h\,\beta l) = x_1, \tag{14}$$

$$\left|1 + \frac{\left(\mathrm{EI}\beta^2\right)^2}{k_T k_R}\right|\left(2\frac{\mathrm{EI}\beta}{k_R}\sin\beta l + \cos h\,\beta l + \cos\beta l\right) = x_2, \tag{15}$$

$$\frac{\mathrm{EI}\beta^3}{k_T}\left\{\left(\cos\beta l + \frac{\mathrm{EI}\beta}{k_R}\sin\beta l\right)\left(\frac{\mathrm{EI}\beta}{k_R}\cos\beta l + \sin h\,\beta l\right) + \left(\sin\beta l - \frac{\mathrm{EI}\beta}{k_R}\cos\beta l\right)\left(\frac{\mathrm{EI}\beta}{k_R}\sin\beta l + \cos h\,\beta l\right)\right\} = x_3, \tag{16}$$

$$\beta^4 = \frac{\rho A\omega^2}{\mathrm{EI}}. \tag{17}$$

In the formula, l is the bolt length, E is Young's modulus, I is the moment of inertia of cross section, A is the cross-sectional area of the bolt, ρ is the density, ω is the frequency, k_T is the bolt transverse spring coefficient, and k_R is the bolt circumferential spring exchange coefficient.

3. Experimental Method and Setup of Bolted Connections

3.1. Test Structure. The experimental structure, as shown in Figure 1, consisted of a bolt, nut, and 42CrMo4 cube with a side length of 35 mm. A through-hole with a diameter of 11 mm was drilled at the center of the specimen, and it was connected using an M10 × 55 bolt. In this experiment, square steel was used as the connecting component to reduce the influence of frictional contact between multiple connected components on the natural frequency and mode shapes of the specimen, thus making the pretightening force testing method more intuitive and accurate. Referring to [18], points 1 to 6 on the specimen represented the locations for impact testing, and the red square on the opposite side of point 6 indicated the installation position of the accelerometer sensor.

3.2. Experimental Device. The experimental setup, as illustrated in Figure 2, consisted of four components: the excitation system, response system, dynamic signal acquisition and analysis system, and computer analysis software. The excitation system primarily referred to the force hammer, while the response system comprised accelerometers, test bolts, and 42CrMo4 square steel components. The dynamic signal acquisition and analysis system used the INV 3018 vibration and noise analyzer developed by COINV, and the computer analysis software used was DASP V11. The basic parameters of the experimental setup are presented in Table 1.

During the setup of the experimental testing system, accelerometers were bonded to the designated positions on the bearing steel using adhesive to prevent any positional changes during the hammering process. The accelerometers were connected to the INV 3018 vibration and noise analyzer, and the force hammer was also connected to the

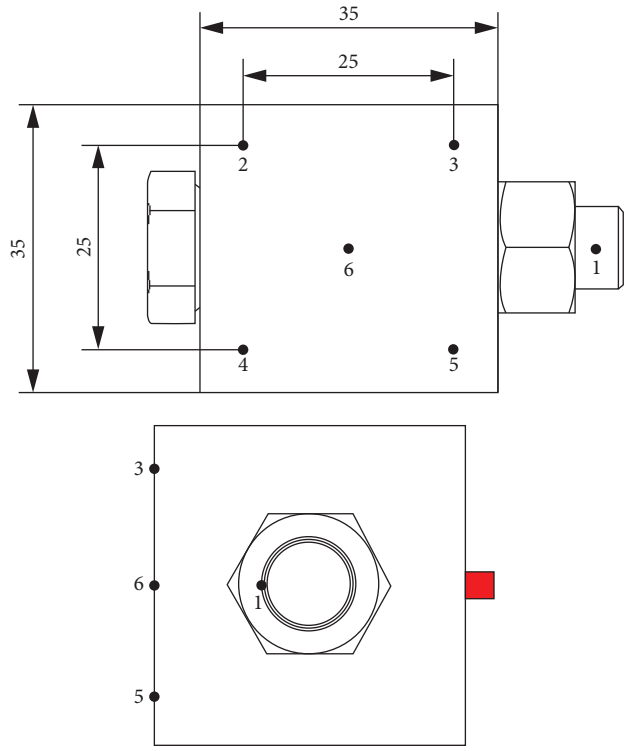

Figure 1: Bolt experimental model.

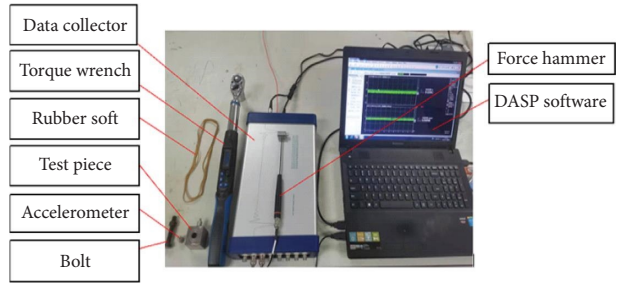

Figure 2: Experimental instrument.

Table 1: Experimental instrument parameters.

Name	Model	Range	Error/calibration value
Bolt	M10 × 55 GB/T152.4-1988	0~60 N·m	—
Accelerometer	INV9824	0~40 kHz	0.525 mV/ms^{-2}
Torque wrench	Electronic digital display	2~60 N·m	±5%
Data acquisition instrument	INV 3018	0~102.4 kHz	—
Force hammer	INV9310	0~500 N	9.97 mV/N

acquisition instrument. Finally, the acquisition instrument was connected to the computer for data collection and analysis.

3.3. Boundary Conditions. The different constraints in experimental conditions could lead to significant differences in the modal test results. In this experiment, the unconstrained condition was adopted because it was easier to simulate compared to the boundary-constrained condition. The rubber ropes were selected as the suspension system on the test platform, as shown in Figure 3, to simulate the free boundary condition. However, due to the presence of rubber ropes, it was not an absolute unconstrained state, and thus there were certain differences between the experimental and numerical simulation results.

The experimental setup utilized the single-reference point test method, which involved fixing an accelerometer at a specific location and moving the force hammer excitation point, as shown in Figure 4. The test points on the specimen (1~6) were sequentially struck, and three impacts were applied at the excitation point. During the hammering process, it was crucial to ensure that the direction of the force

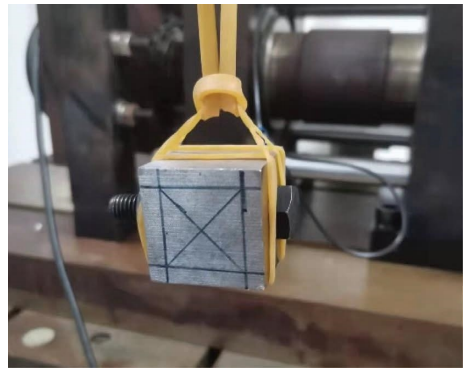

Figure 3: Constraint conditions.

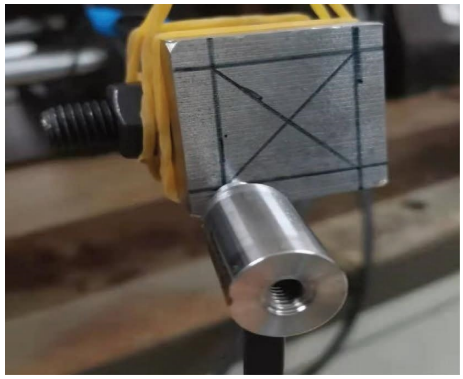

Figure 4: Incentive mode.

the hammer struck was perpendicular to the specimen surface.

Through numerical simulations in the following section, it was determined that the 1st bending mode frequency of the model was around 20 kHz. Therefore, an aluminum force hammer tip was chosen for this experiment.

4. Modal Testing and Simulation

4.1. Experimental Modal Measurement. The application of preloading force in the experimental model of the bolt was achieved by converting torque to preload force based on equation (18). The tightening torque coefficient K varied due to differences in the thread surface finish and lubrication conditions. A surface-plated galvanized bolt of grade 12.9 was selected for the experiment, and no lubrication was applied during tightening. Referring to Table 2, the tightening torque coefficient K was chosen as 0.22. Torque was applied using an electronic torque wrench with a digital display, and the relationship between torque and preload force was obtained by utilizing equation (18), as shown in Table 3.

$$T = \mathrm{K}F_0 d. \tag{18}$$

In the formula, T represents torque, F_0 represents bolt preload, K represents tightening torque coefficient, and d represents nominal diameter.

The data acquisition was conducted with a sampling frequency of 102.4 kHz. The triggering method involved initiating data collection when the impact force of the hammer exceeded 5 N. To capture the complete vibration signal, each sampling cycle was set to include 32,768 data points, with a sampling lag of 256 points. Three trigger events were set for each measurement point. With the aforementioned parameter settings, three hammer strikes were applied to a specific measurement point on the specimen, resulting in a complete set of time-domain vibration acceleration response signals, as shown in Figure 5. The time it took for the acceleration response signal to attenuate to zero after a single excitation was approximately 4 ms, and the signal exhibited a symmetric distribution on both sides, indicating the reliability of the test data. Otherwise, retesting would be necessary after reapplying the hammer strikes.

Table 2: Tightening torque coefficient, K.

Surface state	K value	
	With lubrication	No lubrication
Finishing	0.1	0.12
General processing	0.13~0.15	0.18~0.21
Galvanize	0.18	0.22
Surface oxidation treatment	0.2	0.24

Table 3: Corresponding relationship of torque preload.

T (N·m)	F_0 (N)
5	2272.7
10	4545.5
20	9090.9
30	13636.4
40	18181.8
50	22727.3
60	27272.7

4.2. Modal Simulation of Bolted Connections. The natural frequencies and mode shapes of the bolted connection were determined using finite element analysis. Experimental investigations were conducted to study the influence of varying bolt preloads on the natural frequencies of the specimen and to further validate a modal testing method for evaluating bolt preloads. Because mesh refinement in finite element analysis not only affected the computation time but also impacted the accuracy of the solution, grid-independent analysis was

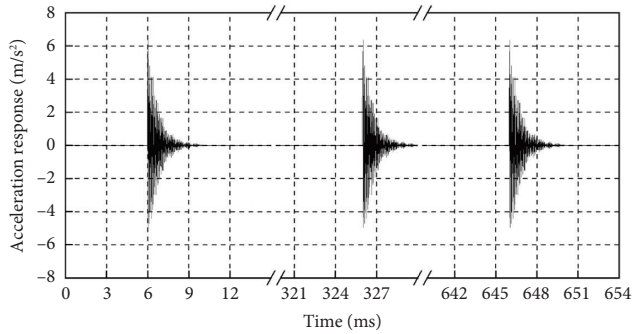

Figure 5: Acceleration response time-domain signal.

conducted. A convergence target value was set, and multiple automatic computations were performed to ascertain a mesh-independent solution using Ansys Workbench.

According to Figure 1, a finite element model consisting of bolts, nuts, and 42CrMo4 square steel was created in Workbench. An allowable change of 0.1% was set. Ansys Workbench automatically refined and solved the finite element model's mesh and compared the results with the previous computations until the allowable change dropped below the set threshold. The computation results are presented in Table 4 and Figure 6. Using the initial model with a unit size of 6 mm, after the first computation of the first-order bending mode frequency, a convergence insert was implemented. Three additional computations were performed. The frequency obtained in the fourth computation was 21992 Hz, with only a 0.038% difference from the third computation result, meeting the convergence requirement.

As shown in Figure 6, it could be observed that the influence of mesh size variation on the 1st mode frequency gradually diminished, approaching convergence. The smallest difference was observed in the fourth computation. However, with the reduction of mesh size, the mesh density and computation time increased substantially, significantly affecting computational efficiency. Considering convergence analysis comprehensively, to ensure a balance between computational accuracy and efficiency, a cubic mesh size of 2 mm was adopted during mesh partitioning. Additionally, to ensure precision in bolt connections, the mesh size for both bolts and nuts was defined as 1 mm, as illustrated in Figure 7. The number of nodes was 85495. Material properties for the 12.9-grade high-strength bolts, nuts, and 42CrMo4 steel were defined according to Table 5.

The finite element model consisted of three contact pairs. The contact between the bolt head and the 42CrMo4 square steel, as well as the contact between the nut and the 42CrMo4 square steel, were defined as bonded contacts. The contact between the bolt and the nut was modeled using the MPC method. The bonded contacts represented the fully loaded state with a bolt preload of 60 N·m. To represent the specimen in a free boundary condition, no additional constraints were added for modal analysis. The modal results were then inputted into the harmonic response analysis module, with an excitation frequency range of 0 to 40 kHz and a modal damping ratio defined as 0.03. A 5 N excitation load was applied at the six measurement points shown in Figure 1 for numerical simulation and solution.

Table 4: Convergent data.

Solution number	Nodes	Elements	1st mode frequency (Hz)	Change (%)
1	1542	388	22286	
2	10067	5940	22114	−0.781
3	69285	46143	22001	−0.515
4	488218	346350	21995	−0.038

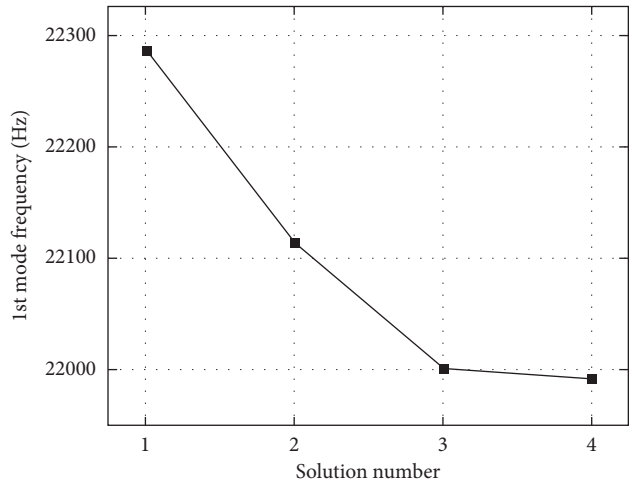

Figure 6: Convergence history.

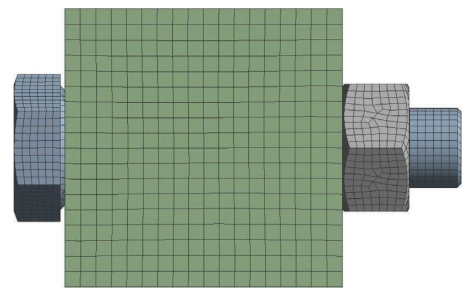

Figure 7: Finite element model.

Table 5: Material properties.

	Young's modulus (GPa)	Poisson's ratio	Density (g/cm^3)
Bolts and nuts	206	0.3	7.82
42CrMo4	210	0.3	7.85

4.3. Natural Frequency and Mode Shape Analysis. The extracted force hammer input signals and acceleration output signals from measurement points 1 to 6 at a bolt preload of 60 N·m were used to calculate the transfer functions. The frequency response functions, coherence, phase, and amplitude were determined, as shown by the

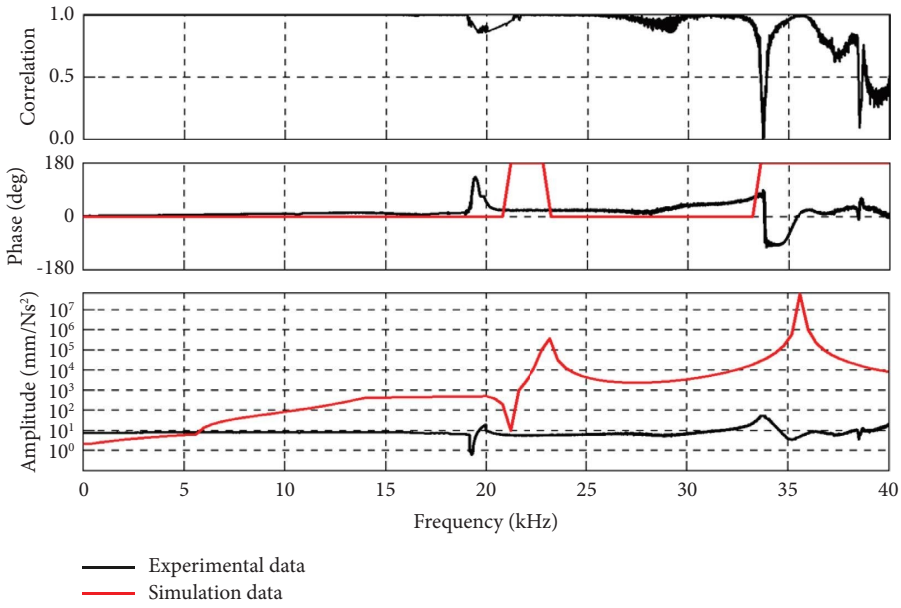

Figure 8: Frequency response function.

Table 6: Natural frequency and vibration mode.

Order	Experiment with the mode shape	Experiment frequency (Hz)	Simulate mode shapes	Simulation frequency (Hz)	Error (%)
1st mode	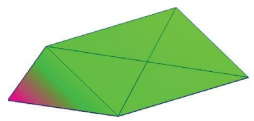	19,881	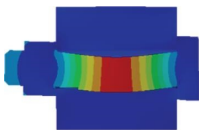	21,995	9.6
2nd mode		19,902	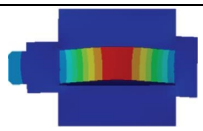	21,996	9.5
3rd mode	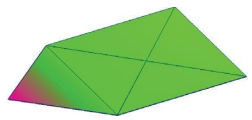	37,789	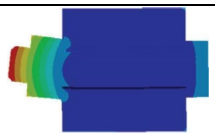	33,683	10.8
4th mode	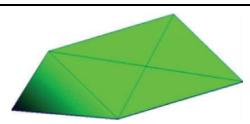	40,827	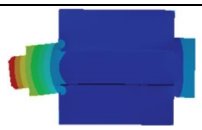	33,732	17.4

black lines in Figure 7, and compared with the results from the finite element analysis. The frequency response functions, phase, and coherence all indicated that the experimental and simulation results exhibited similar trends. However, due to the inability to achieve complete free constraints in the experiment, there was a slight discrepancy between the results.

From Figure 8, it could be observed that the model exhibited two natural frequencies near 20 kHz and 35 kHz, confirming the conclusion of a symmetric model with repeated roots. The extracted natural frequencies and mode shapes from both the experimental and simulation results are shown in Table 5, with the simulation mode shapes referenced to the bolt's central axis as the cross-section.

Based on Table 6, the mode shapes from the experiment and simulation were consistent with each other. The first and second modes were symmetric bending modes, with deformation primarily occurring at the bolt head and the bolt's center position. The third and fourth bending modes showed deformation primarily at the bolt head, with no deformation observed in the connected 42CrMo4 square steel in the first four bending modes. However, the third and fourth bending modes were close to the frequency testing range of the acceleration sensor, resulting in larger errors. Therefore, the

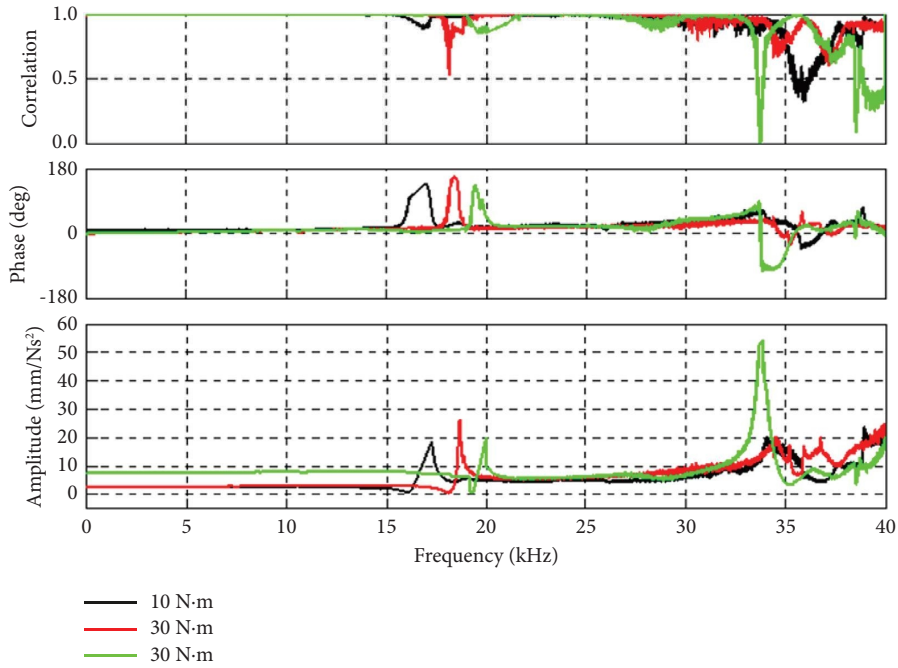

Figure 9: Comparison diagram of the frequency response function.

relationship between natural frequencies and bolt preload will be investigated in the next section based on the first- and second-mode frequencies to determine a method for evaluating preload.

4.4. Evaluation of Bolt Preload Variations. For analysis, experimental data were extracted for bolt torques of 10 N·m, 30 N·m, and 60 N·m. The frequency response functions are shown in Figure 9. It could be seen that as the preload force increased, the coherence, phase, and amplitude of the frequency response function varied around the peak near 20 kHz, indicating an increase in the natural frequency with increasing preload force. Since the model exhibited repeated roots around 20 kHz, there was an overlap between the first bending mode frequency at 60 N·m and the second bending mode frequency at 30 N·m within a certain frequency range. This could lead to ambiguity in evaluating the magnitude of the preload force. Therefore, in this model, the second bending mode frequency was used to assess the bolt preload force.

Torques of 5 N·m, 10 N·m, 20 N·m, 30 N·m, 40 N·m, 50 N·m, and 60 N·m were applied to the bolts, and two modal tests were conducted for each torque level. Five bolts were used for repeated tests, resulting in the corresponding relationship between the second bending mode frequency and the tightening torque as shown in Figure 10. From Figure 10, it could be observed that the bolt frequency was positively correlated with the tightening torque, and the frequency variation range was more pronounced for preloads less than 30 N·m, leading to more accurate preload evaluation. As the tightening torque increased, the frequency variation tended to stabilize, introducing some errors in preload assessment. Therefore, it was feasible to evaluate the trend of preload changes by measuring the variation in the second bending mode frequency of the bolted joint structure. The experiment also demonstrated that different bolts of the same size and model had minimal impact on the structure's natural frequencies.

5. Verification of Applicability of Bolt Preload Evaluation Method

To validate the applicability of the modal method for evaluating preload force, verification was conducted on bolts of different sizes and models, as shown in Table 7. Based on the test results from the previous section, it was observed that bolts of the same model but different sizes exhibited little dispersion in the second bending mode frequency under the same preload force. Therefore, in the experiment of this section, each group of bolts was subjected to three repeated tests, and the average values of the three test results were calculated to obtain the corresponding second bending mode frequencies.

The A~D experiments primarily investigated the applicability of the testing method for different bolt lengths, and the results are shown in Figure 11. From the graph, it could be observed that the bolt length had some influence on the natural frequency but still followed the positive correlation between preload force and the second bending mode frequency. Therefore, this method could be used to evaluate the trend of preload force changes in bolts. It should be noted that for the D bolt, which had a longer length extending beyond the length of the connected component, the second mode frequency exhibited a larger variation range before reaching 10 kN·m.

The bolt connections in wind turbine pitch bearings mainly used grade 12.9 high-strength bolts. In the previous section, the modal preload testing using grade 12.9 high-strength bolts provided consistent results. However, in

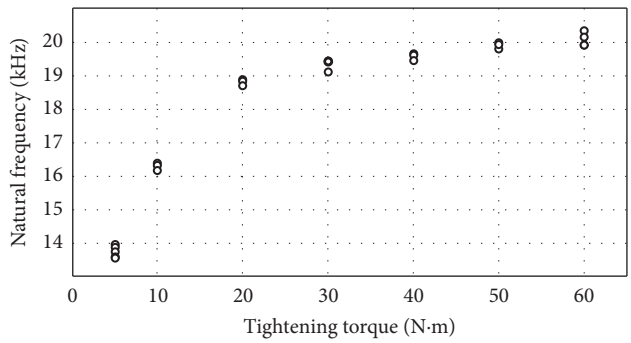

Figure 10: Corresponding relationship between natural frequency and tightening torque.

Table 7: Specifications of bolts of different models.

Test serial number	Nominal diameter	Intensity rating	Screw length	With or without gaskets
A	M10	12.9	50	NO
B	M10	12.9	55	NO
C	M10	12.9	60	NO
D	M10	12.9	65	NO
E	M10	8.8	55	NO
F	M10	4.8	55	NO
G	M10	12.9	55	YES

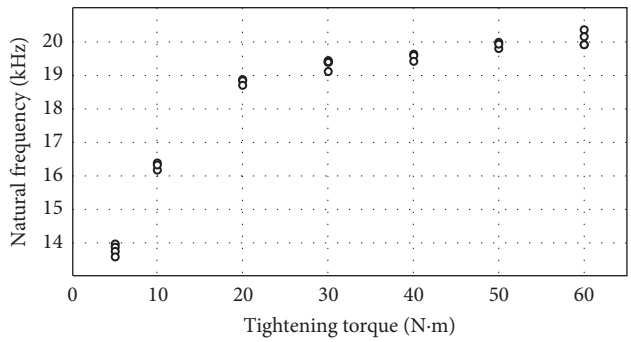

Figure 11: Effect of different screw lengths on second-order bending natural frequency.

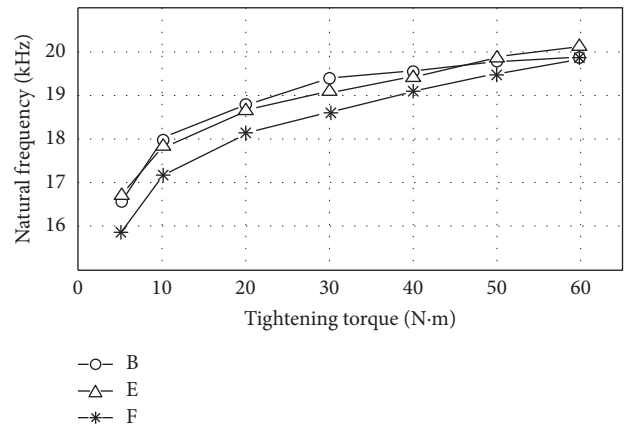

Figure 12: Influence of different strength grades on second-order bending frequency.

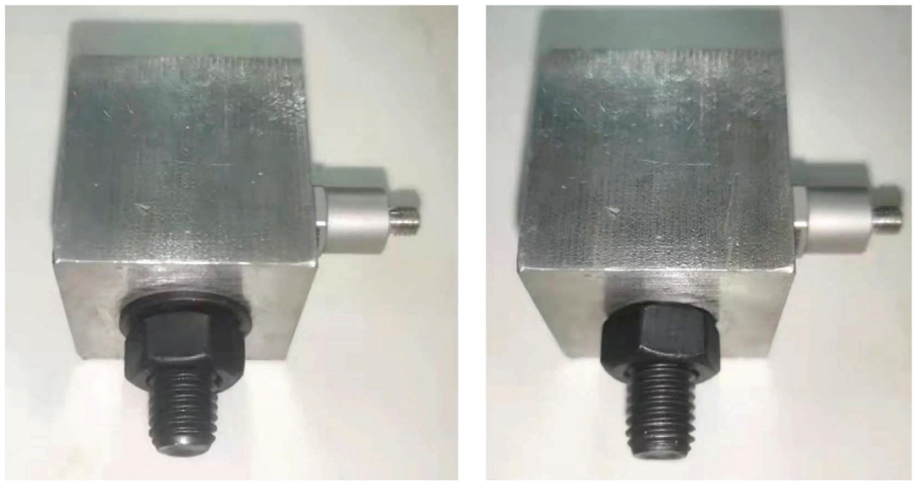

(a) (b)

Figure 13: Comparison diagram of bolt connection with or without gasket. (a) Bolted connection with gasket. (b) Bolted connection without gasket.

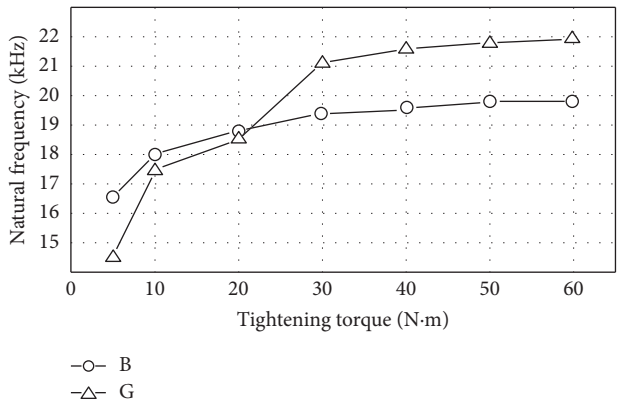

Figure 14: Effect of the gasket on the second-order natural frequency.

engineering applications, grade 8.8 and grade 4.8 bolts are more commonly used. Therefore, it was necessary to validate the applicability of this method for different strength grades. By conducting modal preload tests on B, E, and F bolts, the relationship between preload force and natural frequency was obtained, as shown in Figure 12. The results indicated that, for the three different strength grades of bolts, the second bending mode frequency exhibited similar variations with changes in preload force. Hence, this method was suitable for grade 8.8 and grade 4.8 bolts.

When structural components were bolted together in engineering applications, it was often necessary to place washers between the nut and the connected component. To study the applicability of washers in this method, a washer was added to the G bolt connection, as shown in Figure 13(a), while the B bolt connection was tested without a washer, as shown in Figure 13(b). The influence of the presence or absence of washers on the second bending mode frequency was investigated through modal preload testing using the hammering method. The test results are shown in Figure 14. When washers were used in the bolt connection, the test results aligned with the findings of the previous section. However, the G bolt connection with washers exhibited a higher second bending mode frequency under full load compared to the washerless B bolt connection. At a preload force of 5 kN·m, the G bolt connection with washers showed a lower second bending mode frequency than the washerless B bolt connection, indicating a wider range of second bending mode frequencies for the G bolt connection with washers.

6. Conclusion

This study proposed a vibration modal testing method for evaluating bolt preloading based on modal testing principles. A testing platform for assessing bolt preloading was established, and hammer modal tests were conducted on 42CrMo4 bolted connections of pitch bearings under different preloading conditions. Through numerical simulations and experimental methods, the impact of changes in bolt preloading on natural frequencies and modes was investigated. The study revealed that the first four bending modes of the bolted connection model corresponded to each other. Additionally, by studying frequency response functions under different tightening torques, it was determined that changes in preloading led to alterations in the peak values of coherence, phase, and amplitude in frequency response functions. The fundamental relationship of a positive correlation between bolt preloading and the second-order bending frequency was established. The experiments demonstrated the feasibility of evaluating bolt preloading using the second-order bending frequency of bolted connections and validated the applicability of the hammer modal testing method to bolted connections of different sizes and types.

Nomenclature

K: Stiffness matrix
k_r: The r-th order modal stiffness matrix
N: The total order of structural mode
$H_{ij}(\omega)$: The transfer function of the structure
m_r: Modal mass
Φ_{ri}: The i r-order modal shape of i point
Φ_{rj}: The j r-order modal shape of j point
ω_r: The r-th modal frequency
ξ_r: Damping ratio
l: Bolt length
E: Young's modulus
I: Moment of inertia of the cross-section
A: The cross-sectional area of the bolt
ρ: Density
ω: Frequency
k_T: Bolt transverse spring coefficient
k_R: Bolt circumferential spring exchange coefficient
T: Torque
F_0: Bolt preload
K: Tightening torque coefficient
d: Nominal diameter.

Data Availability

The data used in this study are included within the paper.

Conflicts of Interest

The authors declare that they have no conflicts of interest.

Acknowledgments

This research was funded by the Guangxi Natural Science Foundation of China under grant numbers 2020GXNSFBA297124 and 2021GXNSFAA220038 and the Guangxi Key Research and Development Project of China under grant numbers Guike AB22080008.

References

[1] T. Sun and Z. Wang, "Finite element analysis of contact stress of pitch bearing," *Coal Mine Machinery*, vol. 43, no. 01, pp. 83–85, 2022.

[2] S. Du, "Comparative analysis of different loading modes of wind turbine pitch bearing," *Harbin Bearing*, vol. 40, no. 04, pp. 6–9, 2019.

[3] M. Xu and G. Wu, "Research on wear resistance technology of wind turbine pitch bearing cage," *Harbin Bearing*, vol. 41, no. 03, pp. 9–12, 2020.

[4] Y. Tong, B. Zhu, D. Xu et al., "Research on the control method of the pre-tightening accuracy of the connecting bolts of the pitch bearing of the wind turbine generator," *Mechanical Design and Manufacturing Engineering*, vol. 51, no. 06, pp. 88–92, 2022.

[5] C. Wang, L. Guo, L. Fu, and J. Liu, "High-power wind power is analyzed.studying bearing test technique," *Bearing*, pp. 1–5, 1974.

[6] H. J. McFaul, "An ultrasonic device to measure high-strength bolt preloading," *Materials Evaluation*, vol. 32, pp. 244–248, 1974.

[7] M. Suda, Y. Hasuo, A. Kanaya, Y. Ogura, T. Takishita, and Y. Suzuki, "Development of ultrasonic axial bolting force inspection system for turbine bolts in thermal power plants," *JSME international journal. Ser. 1, Solid mechanics, strength of materials*, vol. 35, no. 2, pp. 216–219, 1992.

[8] A. Koshti, "Ultrasonic measurement of the bending of a bolt in a shear joint," *Experimental Mechanics*, vol. 38, no. 4, pp. 270–277, 1998.

[9] K. Y. Jhang, H. H. Quan, J. Ha, and N. Y. Kim, "Estimation of clamping force in high-tension bolts through ultrasonic velocity measurement," *Ultrasonics*, vol. 44, no. 8, pp. 1339–1342, 2006.

[10] H. Yasui, H. Tanaka, I. Fujii, and K. Kawashima, "Ultrasonic measurement of axial stress in short bolts with consideration of nonlinear deformation," *JSME International Journal Series A*, vol. 42, no. 1, pp. 111–118, 1999.

[11] S. Chaki, G. Corneloup, I. Lillamand, and H. Walaszek, "Combination of longitudinal and transverse ultrasonic waves for in situ control of the tightening of bolts," *Journal of Pressure Vessel Technology*, vol. 129, no. 3, pp. 383–390, 2007.

[12] N. Kim and M. Hong, "Measurement of axial stress using mode-converted ultrasound," *NDT & E International*, vol. 42, no. 3, pp. 164–169, 2009.

[13] X. Ding, X. Wu, and Y. Wang, "Bolt axial stress measurement based on a mode-converted ultrasound method using an electromagnetic acoustic transducer," *Ultrasonics*, vol. 54, no. 3, pp. 914–920, 2014.

[14] B. Blachowski, A. Swiercz, P. Gutkiewicz, J. Szelążek, and W. Gutkowski, "Structural damage detectability using modal and ultrasonic approaches," *Measurement*, vol. 85, pp. 210–221, 2016.

[15] J. S. Heyman, "A CW ultrasonic bolt-strain monitor: a new sensitive device is reported for the measurement of stress-related strain as well as stress-related change in velocity of sound," *Experimental Mechanics*, vol. 17, no. 5, pp. 183–187, 1977.

[16] S. G. Joshi and R. G. Pathare, "Ultrasonic instrument for measuring bolt stress," *Ultrasonics*, vol. 22, no. 6, pp. 261–269, 1984.

[17] M. Hirao, H. Ogi, and H. Yasui, "Contactless measurement of bolt axial stress using a shear-wave electromagnetic acoustic transducer," *NDT & E International*, vol. 34, no. 3, pp. 179–183, 2001.

[18] N. Hosoya, T. Niikura, S. Hashimura, I. Kajiwara, and F. Giorgio-Serchi, "Axial force measurement of the bolt/nut assemblies based on the bending mode shape frequency of the protruding thread part using ultrasonic modal analysis," *Measurement*, vol. 162, Article ID 107914, 2020.

[19] A. Khomenko, E. G. Koricho, M. Haq, and G. Cloud, "Bolt tension monitoring with reusable fiber bragg-grating sensors," *The Journal of Strain Analysis for Engineering Design*, vol. 51, no. 2, pp. 101–108, 2015.

[20] S. Ritdumrongkul, Y. Fujino, and M. Asce, "Identification of the location and level of damage in multiple-bolted-joint structures by PZT actuator-sensors," *Journal of Structural Engineering*, vol. 132, no. 2, pp. 304–311, 2006.

[21] J. Shao, T. Wang, H. Yin, D. Yang, and Y. Li, "Bolt looseness detection based on piezoelectric impedance frequency shift," *Applied Sciences*, vol. 6, no. 10, p. 298, 2016.

[22] K. Huang, "Jin Jianxin Research on bolt pre-tightening force simulation based on the virtual material method," *Mechanical Design and Manufacturing*, vol. 8, no. 3, pp. 148–150, 2012.
[23] Z. Gong, B. Wang, and G. Yu, "Study on the influence of bolt pre-tightening force on the characteristic parameters of bolt joint surface," *Mechanical strength*, vol. 40, no. 2, p. 6, 2018.
[24] G. Zhao, Z. Xiong, X. Jin, L. Hou, and W. Gao, "Prediction of contact stiffness in bolted interface with natural frequency experiment and FE analysis," *Tribology International*, vol. 127, pp. 157–164, 2018.
[25] Y. Zhang, *Research on Identification Method of CFRP Lap Plate Bolt Looseness Based on Modal Analysis and RBF Neural Network*, Jinan: Jinan University, Guangzhou, China, 2020.
[26] L. Hou, *Dynamic Modeling and Application of Bolted Connection Considering Contact Damping*, Dalian: Dalian University of Technology, Dalian, China, 2020.
[27] M. Okugawa and K. Egawa, "Study on smart washer using piezoelectric material for bolt loosening detection," *JSNDI*, vol. 52, pp. 511–516, 2003.
[28] Y. Yunshu, *Structural Modal Test Analysis*, Astronautics Publishing House, Reston, VA, USA, 2000.